Modeling and Analysis of a Fast and Robust Module-Integrated Analog Photovoltaic MPP Tracker

Somnath Maity, *Member, IEEE*, and Pradeep Kumar Sahu

***Abstract*—Analog circuitry-based photovoltaic (PV) maximum power point (MPP) tracking (MPPT) technique is attractive due to its low cost and capability of easy integration with normal dc–dc switching converters. However, realization of classical digital MPPT algorithms using analog circuitries is a challenging task. It necessarily requires to store the information of module voltage/current and power in order to find the desired MPP. While at the same time, improper design of digital MPPT controllers may cause poor tracking performances or limit cycle oscillations to manifest, which are generally seen as being undesirable. This paper proposes a fast and robust analog PV MPP tracker without imposing any external control or perturbation. The fast dynamic performances with absolute robustness are ensured here by integrating the concepts of Utkin's equivalent sliding mode control law and fast-scale stability analysis of actual switched converter systems. Moreover, the superiority of the proposed MPP tracker (in terms of high-tracking performances) over classical ones, and its impact in series-connected converters configuration are analytically demonstrated through the procedure developed in this paper. Finally, the analytical results have been validated by means of simulations and experiments.**

***Index Terms*—Analog controller, maximum power point tracking (MPPT), photovoltaic (PV) systems, sliding mode control (SMC), stability analysis.**

I. Introduction

In typical residential photovoltaic (PV) applications, PV systems are composed of a number of series-connected modules arranged in parallel, and they usually suffer from a current mismatch between different modules due to manufacturing variability, dirt accumulation, or partial shading of the array [1]. In this architecture, any source of cell current mismatch or nonuniform shading will cause the overall system output power to be reduced since the current in the string is limited by the weakest module. While modules used today typically employ bypass diodes that limit the negative effect of partial shading and help protect the panels [2], it is still the case that shading effect has a significant negative impact on any solar PV installations. The module-integrated converter (MIC), the so-called microconverter concept has been exploited to address this problem by operating each module at its unique maximum power point (MPP) and providing separate dc–dc conversion for each module [3]–[5]. Through dc–dc converters, localized control of module current and voltage can be achieved, and each module can operate at its independent MPP to improve the energy extraction of the overall system.

However, designing a fast and robust PV MPP tracking (MPPT) controller (with high-tracking efficiency) for such MIC is a challenging task for power electronics practitioners [6]. Over the past decades, many efforts have been devoted to this research area and reviews are available now on this subject [6]–[9] and references therein. In most of the cases, investigations are primarily based on standard perturb and observe (P&O) algorithms, constant-frequency (CF) pulse width modulated (PWM) operation, and small-signal averaging technique or transfer function-based stability analysis. However, averaging is only an approximated procedure to obtain the low-frequency behavior of the actual switching model of the dc–dc converters. The averaged model was failed to predict many fast-scale instabilities (e.g., subharmonic oscillations and chaotic behavior) that may develop in the current and voltage waveform at clock frequency, causing high conduction loss, and excessive switching stress [10]. This shortcoming is due to elimination of the discontinuous effect of the real converter system and ignoring the microscopic dynamics inside the switching cycle (see [11] and references therein), as well as the quantization effects [12], which is inherently induced in all digitally controlled MPPT systems [13]. Because of this approximation, the traditional use of averaging-based analysis technique and also P&O algorithm cannot always extract the best optimized performances in terms of fast and robust dynamic performances, steady-state oscillations, and tracking efficiency. The optimized performances of P&O-based MPPT controller depend largely on amplitude and frequency of the perturbations applied to the switching converter [14]. It is therefore necessary to apply a more advanced controller, as well as the fast-scale stability analysis technique (bifurcation analysis) in order to achieve such specific performances.

It has, however, been recently reported that dynamic responses of a MPP tracker can be improved by combining the different mode of controllers like sliding and constant-frequency PWM [15] or hysteresis controller [16]–[19] with relatively costly A/D and D/A converters. As a consequence of this combination, the sliding mode controller (SMC) essentially utilizes a CF-switching (CFS) control law to force the state trajectory from any initial position onto a specified surface in the state space, called the switching or sliding surface (SS), and maintain it on this surface for all subsequent time. The main features of the *ideal* sliding mode (SM) are the robustness against the parameters fluctuations. Despite these unique advantages of ideal one, the controllers reported earlier completely rely on smooth averaged models of the dc–dc switching converters

Manuscript received September 17, 2014; revised December 14, 2014; accepted February 1, 2015. Date of publication February 10, 2015; date of current version September 21, 2015. This work was supported in part by the DST, Govt. of India under Indo-Taiwan Joint Research Programme (File No.: GITA/DST/TWN/P-58/2014). Recommended for publication by Associate Editor C. A. Canesin.

The authors are with the Department of Electrical Engineering, National Institute of Technology, Rourkela, Orissa 769008, India (e-mail: somnathm@nitrkl.ac.in; pksahu.nitrkl@gmail.com).

Color versions of one or more of the figures in this paper are available online at http://ieeexplore.ieee.org.

Digital Object Identifier 10.1109/TPEL.2015.2402281

and the control is only valid on a reduced-order SS. However, in real-life power electronics converter systems, SM actually occurs not on its discontinuity surface, but within the vicinity of that discontinuity or within a boundary layer surrounded by multiple-switching surfaces, like hysteresis control [16]–[19]. In such situation, the control components may take up values, which are different from the equivalent control law; therefore, result in a richer set of motions on the sliding manifold [20]. The existence of a unique sliding motion can only be determined successfully using the notion of Utkin's equivalent control or Filippov continuation method if the fast-scale dynamics is stable. The mathematical proof of this concept has already been developed earlier in multiscale hybrid dynamical systems (HDSs) [21]. Since the switching converters used in PV systems come under this class of systems [11], [22], the equivalent equation of motion derived from Utkin's theory may not be always successful to predict the existence of a unique solution or robustness. It can only be successfully used when the long-time averaging of fast-scale oscillations becomes zero, in other words, when the capacitor voltage and the inductor current waveforms during the steady-state operation are periodic in nature [21].

In view of this, this paper proposes a fast and robust analog-MPP tracker [also called as analog sliding-mode controller (ASMC)], which is implemented and designed by using the concepts of Utkin's equivalent control theory and fast-scale stability analysis. The main objectives of applying such concepts are to provide the control support for the MPPT system, which are required for 1) guaranteed stability with high robustness against the parameters uncertainties, and 2) fast dynamic responses under rapidly varying environmental conditions. This cannot be met by conventional digital or analog MPPT controllers without continuously tuning the controller parameters and complex controller architecture [6], [23]. Thus, the choice of this analog solution is quite attractive because of its low cost and capability of easy integration with a normal dc–dc converter in integrated circuit (IC) form so that plug-and-play operation for many low-power residential PV applications [3], [24] can be easily achieved. Moreover, since the proposed analog controller inherently acts like a CF hysteresis controller [16], [17], it retains all of the properties of an *ideal* SMC, that is, simplicity in practical realization, good dynamic response with high robustness, and less overshoot in the output module voltage. In addition, it provides a relatively larger bandwidth to eliminate the low-frequency limit cycle oscillation [13], and reduces the cross-coupling effects, which is normally occurred in series-connected converters systems [25].

To explore the above issues, the paper is organized as follows. First, in Section II, a brief review of proposed analog MPPT technique and its switching dynamics is discussed. Based on this discussion, a modular PV system (MPVS) is analyzed by using the concepts of Utkin's equivalent control law and fast-scale stability analysis in Section III. In particular, this section explores how the method of analysis and design of MPVS can play the strategic role for characterizing the fast and robust dynamic performances. Finally, the performances are experimentally verified and compared numerically with the classical P&O algorithm in Section IV.

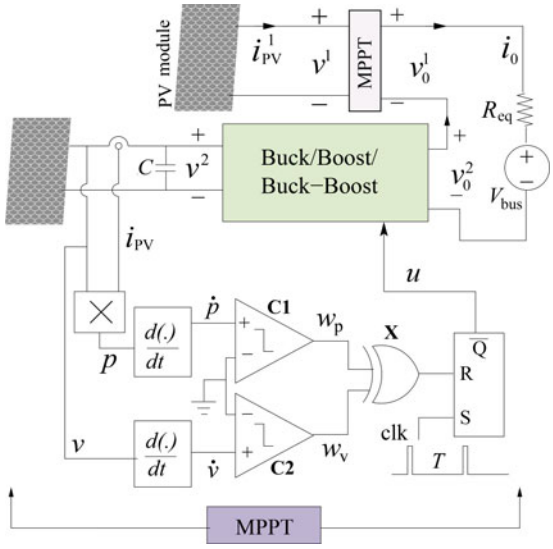

Fig. 1. Schematic showing the series architecture with a string of two MPVS and zooming view of analog MPP tracker.

II. Glimps at Module-Integrated Analog MPP Trackers

In this section, the architecture shown in Fig. 1 is considered in order to introduce the proposed modular MPP trackers. It consists of two PV modules which are interconnected with two nonautonomous switching converters, and each of them comprising of an input capacitor C, a low-pass filter with inductor L and capacitor C_o, a diode D, and a controllable switch S, governed by an analog MPPT controller without imposing any external control or perturbation. The output of the dc–dc converters is connected in series and put in parallel to the dc bus (input of a dc–ac converter), represented by means of a Thevenin model [18], [26]. Mathematically, the output voltage $V_{\rm bus}$ and corresponding throughput power $P_{\rm o}$ of such series-connected converters system can be expressed as a sum of all modular MPPT controllers [4], [27], such that

$$V_{\rm bus} \approx \sum_{k=1}^{2} v_{\rm o}^{k} \;\text{ and }\; P_{\rm o} = i_{\rm o} \sum_{k=1}^{2} v_{\rm o}^{k};\;\text{ since }\; R_{\rm eq} \approx 0. \quad (1)$$

Here, $i_{\rm o}$ is the averaged load current and $v_{\rm o}^{k}$ is the output voltage of the kth dc–dc converter, which is dynamically coupled with other converters' output voltage. In a system like (1), every disturbance induced on the output voltage, by the other MPVSs and/or by the inverter, directly propagates on the modules' output voltage. This may lead to instability or dynamic performance degradation [25], [27], [28]. In [28], authors demonstrated that if the MPPT controller is fast enough, any disturbances in the closed-loop system do not significantly affect the operation of a single MPVS. This is also true for inverter system. Since fast controller with larger loop-gain has better output disturbance rejection capability than that of slower one [29], therefore, it can avoid the propagation of low-frequency perturbation to the PV module side (see [30]). However, this mandatory requirement makes the achievement of a fast and stable controlled converter

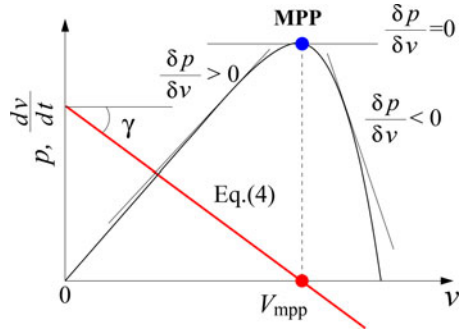

Fig. 2. Representative characteristics of $\dot{v}$ making $V_{\rm mpp}$ as an attractor.

system (in terms of fast- and slow-scale stability), which is really a difficult task.

This paper thus promises to deal the complete stability analysis of proposed analog MPVS in order to achieve fast and robust dynamic responses. The system under this control logic is excellent in tracking effectiveness and rapid dynamic responses [31]. In addition, it inherently makes the MPP as an attractor of the system. Irrespective of any initial voltage, the controller always forces the system's state trajectories to travel toward the MPP satisfying the conditions (see Fig. 2)

$$\frac{\partial p}{\partial v}=\begin{cases}>0 & \text{if} \quad (v-V_{\rm mpp})<0\\ =0 & \text{if} \quad (v-V_{\rm mpp})=0\\ <0 & \text{if} \quad (v-V_{\rm mpp})>0\end{cases} \tag{2}$$

where v is the PV module output voltage, p is the module power, and $V_{\rm mpp}$ is the voltage corresponds to MPP $P_{\max}$. The conditions (2) ensure that depending on the value of power gradient $\partial p/\partial v$, the voltage across the input capacitor v will be increased or decreased toward $V_{\rm mpp}$. If $v<V_{\rm mpp}$, then its rate of change should be positive. Otherwise, if $v>V_{\rm mpp}$, then v is forced to fall and, hence, its rate change should be negative. But if $v=V_{\rm mpp}$, the voltage v is held fixed. The rate of change of v should be zero. The simplest functional form that would confirm these objectives, i.e.,

$$\frac{dv}{dt}=\begin{cases}>0 & \text{if} \quad (v-V_{\rm mpp})<0\\ =0 & \text{if} \quad (v-V_{\rm mpp})=0\\ <0 & \text{if} \quad (v-V_{\rm mpp})>0\end{cases} \tag{3}$$

can be expressed in terms of dv/dt as follows:

$$\frac{dv}{dt}=-\gamma(v-V_{\rm mpp}) \tag{4}$$

where γ is the positive number associated with dynamic response of the controller [31]; the larger the γ, the faster the dynamic response.[1] The graphical representation of (4) is shown in Fig. 2. It is observed that because (2) and (3) have similar forms, a simple control law can be deducted by making

$$\dot{v}\propto\frac{\partial p}{\partial v}=\alpha\frac{\partial p}{\partial v} \tag{5}$$

[1]However, any function complying with (3) would fulfill the objective of (2) and (3), which are indeed in similar forms.

where $\alpha>0$ is a constant. Now, after substituting (5) into expression $\frac{dp}{dt}=\frac{\partial p}{\partial v}\frac{dv}{dt}$ and using the switching logic (2) and (3), one can easily obtain the control law $\frac{\partial p}{\partial v}=\dot{p}/\dot{v}$ having the control algorithm $\dot{v}=\alpha\dot{p}/\frac{\partial p}{\partial v}=\alpha\dot{p}/\dot{v}$, which has to be realized here.

In practice, the realization of such an algorithm $\dot{v}=\alpha\dot{p}/\dot{v}$ is slightly difficult due to presence of an algebraic loop. Since v appears on both sides, it would manifest high-frequency oscillation. One requires an analog divider circuit which is again undesirable. Moreover, divider circuit causes many other imperfect operations and even singularity problem when v becomes zero (in this case, it happens only when $v=V_{\rm mpp}$). While by rearranging the desired control algorithm into the form $\dot{v}^2=\alpha\dot{p}$ does not help either. In fact, squaring of v not only destroys the vital information of its sign, but also causes the singularity problem at MPP. Lim and Hamill [31] showed that the problem of singularity can be resolved by redefining the above control law $\frac{\partial p}{\partial v}=\dot{p}/\dot{v}$ as

$$\frac{\partial p}{\partial v}:=\text{sign}(\dot{p}/\dot{v})\equiv\frac{\text{sign}(\dot{p})}{\text{sign}(\dot{v})}\equiv\text{sign}(\dot{p})\text{sign}(\dot{v}) \tag{6}$$

$$\Rightarrow\text{sign}(\dot{v})=\text{sign}(H)=\begin{cases}+1 & \text{if} \quad H<0\\ -1 & \text{if} \quad H>0.\end{cases} \tag{7}$$

Here, the expressions ((6)) and (7) indicate that in-spite of zero-division the nonlinear function sign(.)/sign(.) can be reformulated as a function of multiplication $G(.)=\text{sign}(.)\text{sign}(.)$, which are realized by a couple of comparators $\mathbf{C_1}$, $\mathbf{C_2}$ followed by an exclusive-OR gate $\mathbf{X}$ [see Fig. 1(b)]. The comparators are used to evaluate the sign of $G(.)$ by producing binary signals (w_p, w_v) whose value is 0 if $\dot{p}<0$ or 1 if $\dot{p}>0$; or, 0 if $\dot{v}<0$ or 1 if $\dot{v}>0$. Multiplication of these binary signals using X-OR gate is further used to generate required switching signals of the control law (7). It essentially contains the information whether v should be increased or decreased to approach MPP. Since sign(.) function in (7) has a discontinuity at the MPP, one cannot expect an equilibrium point at a steady state, rather the system dynamics is governed by very high switching frequency. This results in excessive switching losses and also reduces the life-time of the semiconductor devices.

Although such high switchings can be easily restricted by incorporating latch circuit into the controller, but its presence makes single discontinuity switching surface H into a CFS Δ-neighborhood chatter box, or switching box $S_B=\{v: V_{\rm mpp}-\Delta\le v<V_{\rm mpp}+\Delta;\ t<T, \Delta>0\}$, surrounded by multiple SSs $H=(v-V_{\rm mpp})$ and external clock pulse having time period T. The switching flow diagram of such control algorithm is shown in Fig. 3. It represents that depending on the initial value of the input capacitor voltage $v(0)$, MIC may operate into two modes: one when v is outside the boundary layers and the other when it is inside. At the beginning of every clock pulse, we determine whether the capacitor voltage $v_n=v|_{t=nT}$ (n is a positive integer number) is within the boundary of S_B or not. If it is inside, at start of the clock period $u=0$, i.e., the switch S is turned OFF, capacitor voltage v raises. When v reaches a peak value $V_{\rm mpp}$, $u=1$, i.e., the S is turned ON.

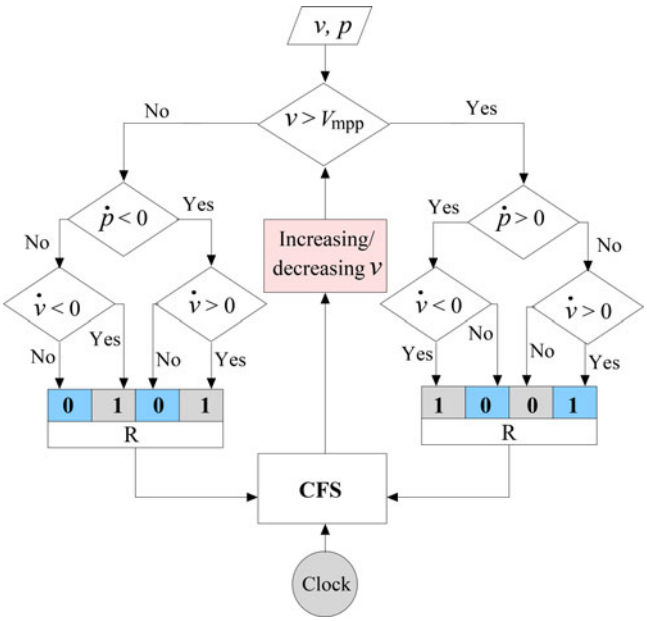

Fig. 3. Switching flow diagram of proposed ASMC.

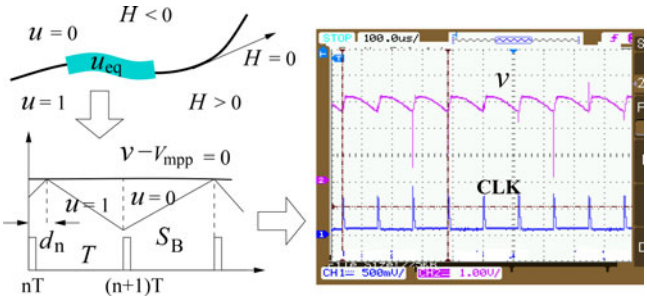

Fig. 4. Hysteretic flow of buck-type MIC for $i_o = 4.8$ A. The other parameters value used are given in Table I.

The input voltage v then starts falling and follows the same dynamics until next clock pulse is arrived. While if v_n is outside of S_B, the switch S is turned ON when $V_{\rm mpp} < v_n$ and turned OFF when $v_n < V_{\rm mpp}$.

Hence, for an arbitrary initial position the controller

$$u = \left\{ \begin{array}{ll} 1, & H < 0 \\ 0, & H > 0 \\ u_{\rm eq} & \text{if } v \text{ is inside} \end{array} \right\} \text{if } v \text{ is outside} \tag{8}$$

drives the trajectories to reach into S_B in finite time $t_s > 0$. Once they reach, a hysteritic flow inside the switching box starts, and an equivalent motion continues to move toward the steady-state periodic orbit rather than equilibrium point. The representative diagram of (8) and corresponding hysteritic flow of the buck-type switching converter, for example, is shown in Fig. 4.

III. SMC MPVS

In the past, it has been reported that the equivalent motion of HDSs (characterized by piecewise smooth system with right-hand side discontinuities) can be determined successfully by using the notion of Utkin's equivalent control or Filippov continuation method [20]. For a single discontinuous SS, there exists a unique solution of equivalent dynamics and the sliding motion obtained from these methods are the same. However with boundary layers control (8), the sliding motion inside the chattered-box only exists when the fast-scale dynamics is stable [11], [21]. In this case, when the fast-scale oscillations of the input capacitor voltage ripple inside S_B are periodic.

TABLE I
SPECIFICATION OF ASMC BASED MODULAR PV SYSTEM FOR $G = 1000$ W/m^2, AND $T_c = 25\,^\circ$C

Converter	PV array
$L = 1.0$ mH, $C = 100\,\mu$F, $C_0 = 1000\,\mu$F $T = 20\,\mu$s	$I_{\rm sc} = 3.8$ A, $V_{\rm oc} = 21.1$ V, $K_V = -0.80$ V/K, $K_I = 0.0065$ A/K $V_{\rm mpp} = 17.1$ V, and $I_{\rm mpp} = 3.5$ A.

A. Existence Conditions Under Ideal Switching Surface

Based on the aforementioned concepts, the analysis and design of proposed MPVS are investigated. The investigations are performed on the basis of full-order state-space model of MIC system [25], [26] and an ideal SSs $H := \partial p/\partial v = 0$ (where $\Delta \to 0$). From dynamical system point of view, MICs operating in continuous-conduction-mode (CCM) can be characterized by sets of 3-D differential–algebraic equations (DAEs) with right-hand side discontinuity (for details, see Table II) as

$$\frac{dx}{dt} = f + gu = \left\{ \begin{array}{ll} f_1 & \forall\, u = 0 \\ f_2 & \forall\, u = 1 \end{array} \right. \tag{9}$$

where u is the discontinuous control signal governed by (8). While the nonlinear PV array current $i_{\rm pv}(x_1)$ is defined as

$$i_{\rm pv}(x_1) = I_{\rm sc} - I_{\rm sat}\left[\exp\left(x_1/aV_T\right) - 1\right] \tag{10}$$

with panel saturation and short-circuit current $I_{\rm sat}$ and $I_{\rm sc}$, diode ideality constant a, and thermal voltage V_T with series and parallel resistance $r_s \approx 0$, $r_p \approx \infty$, respectively. Having obtained the system description (9), next step is to design the controller, so that, control law u will direct the state trajectory towards the desired operation. In this case, it is appropriate to have a SMC law (8) that will adopt the switching function H, defined by

$$H := \frac{\partial p}{\partial x_1} = i_{\rm pv}(x_1) - \frac{x_1 I_{\rm sat}}{aV_T}\exp\left(\frac{x_1}{aV_T}\right) = 0. \tag{11}$$

The objective is that, from any arbitrary initial position $x(0)$, it will drive the system trajectory on either side of the SS $H = 0$. The trajectory is said to be in sliding mode if the motion within the vicinity of H is maintained and consequently directed toward the steady-state equilibrium point. In other words, it can also be stated that SMC is performing its control decision by utilizing the sliding plane $H = 0$ as a reference path, on which trajectory will be attracted and eventually converged toward the equilibrium to achieve the desired steady-state operation satisfying the inequality conditions

$$\lim_{H\to 0^+} \frac{dH}{dt} < 0 \quad \text{and} \quad \lim_{H\to 0^-} \frac{dH}{dt} > 0. \tag{12}$$

TABLE II
DYNAMICS OF ALL THREE MIC ARCHITECTURES AND THEIR REPRESENTATION IN THE FORM OF: $\frac{dx}{dt} = f + gu$, WHERE $x = [v \;\; i \;\; v_o]^T$

Buck converter	Boost converter	Buck–boost converter
$\dot{x}_1 = \frac{i_{\rm pv}(x_1)}{C} - \frac{x_2}{C}u$	$\dot{x}_1 = \frac{i_{\rm pv}(x_1)}{C} - \frac{x_2}{C}$	$\dot{x}_1 = \frac{i_{\rm pv}(x_1)}{C} - \frac{x_2}{C}u$
$\dot{x}_2 = \frac{x_1}{L}u - \frac{x_3}{L}$	$\dot{x}_2 = \frac{x_1}{L} - \frac{x_3}{L}(1-u)$	$\dot{x}_2 = \frac{x_1}{L}u + \frac{x_3}{L}(1-u)$
$\dot{x}_3 = \frac{x_2}{C_0} - \frac{x_3 - i_0}{C_0}$	$\dot{x}_3 = \frac{x_2}{C_0}(1-u) - \frac{x_3 - i_0}{C_0}$	$\dot{x}_3 = \frac{x_2}{C_0}(u-1) - \frac{x_3 - i_0}{C_0}$
$f = \left[\frac{i_{\rm pv}(x_1)}{C} \quad -\frac{x_3}{L} \quad \frac{x_2}{C_0} - \frac{x_3 - i_o}{C_0}\right]^T$	$f = \left[\frac{i_{\rm pv}(x_1) - x_2}{C} \quad \frac{x_1 - x_3}{L} \quad \frac{x_2}{C_0} - \frac{x_3 - i_o}{C_0}\right]^T$	$f = \left[\frac{i_{\rm pv}(x_1)}{C} \quad \frac{x_3}{L} \quad -\frac{x_2}{C_0} - \frac{x_3 - i_o}{C_0}\right]^T$
$g = \left[-\frac{x_2}{C} \quad \frac{x_1}{L} \quad 0\right]^T$	$g = \left[0 \quad \frac{x_3}{L} \quad \frac{x_2}{C_0}\right]^T$	$g = \left[-\frac{x_2}{C} \quad \frac{x_1 - x_3}{L} \quad -\frac{x_2}{C_0}\right]^T$

The conditions (12) are known as the SM reachability or existence conditions [17], [32]. For an ideal SM-controlled MICs, these conditions can be easily derived from the time derivative of SS $\frac{dH}{dt} = \nabla H \frac{dx}{dt}$ and then substituting this value into (12). From (11), ∇H can be evaluated as

$$\nabla H = \left[x_1 \frac{\partial^2 i_{\rm pv}}{\partial x_1^2} + 2\frac{\partial i_{\rm pv}}{\partial x_1} \; 0 \; 0\right] = [F(x_1) \quad 0 \quad 0]$$

where

$$F(x_1) = \left[-\frac{I_{\rm sat}(2aV_T + x_1)}{(aV_T)^2}\exp\left(\frac{x_1}{aV_T}\right) \quad 0 \quad 0\right]$$

is only a function of PV module voltage with nonzero steady-state value. Substituting it into (12), and using (9) and (11) one can easily obtain the boundary conditions for both buck and buck–boost converters as

$$\mathbf{\Pi}_1 := i_{\rm pv} - x_2 < 0 \quad \text{and} \quad \mathbf{\Pi}_2 := i_{\rm pv} > 0. \tag{13}$$

While for boost converter, it can be obtained as

$$\mathbf{\Pi}_1 := i_{\rm pv} - x_2 < 0 \quad \text{and} \quad \mathbf{\Pi}_2 := i_{\rm pv} - x_2 > 0. \tag{14}$$

The conditions (13) and (14) are essentially interpreted as a region requirement for the system trajectories to be oriented toward the sliding surface H from both sides. It is called as a stable region. In that region, two vector fields f_1 and f_2 of (9) are pushing in opposite directions, so that states of the system x are forced to stay on the boundary and slide on it. While in case of an unstable region (i.e., if (13) or (14) does not satisfy) there will be a switching. The trajectories in one state-space region $H < 0$ approaching transversely the switching boundary $H = 0$, cross it and enter into the adjacent region $H > 0$. The representative diagram of all possible trajectory evolutions of three switching converters is shown in Fig. 5. It is important to note that, due to lack an existence region of the boost converter (14), trajectory (denoted by **A**) starting from any initial position travels toward the equilibrium point. Around that point, it starts oscillating in between two neighboring state-space regions with low-frequency switchings and slightly high ripple magnitude. It can, however, be greatly improved by directly sensing of the inductor current (see trajectory **A** in Fig. 5). As discussed in

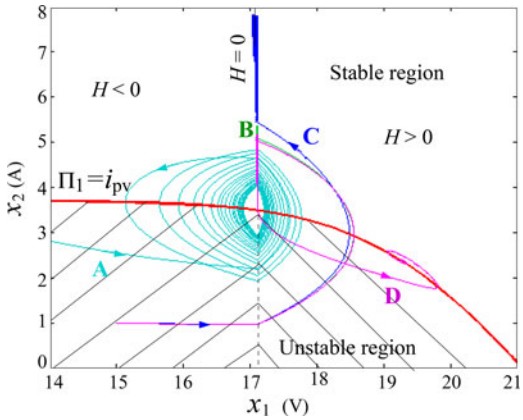

Fig. 5. Trajectory evolution of ASMC-based MPVS showing the switching and sliding motion for $G = 1000$ W/m^2, $T_c = 25\,^\circ$C, and $i_o = 4.8$ A. The other parameters value used are given in Table I.

[33], MPPT technique employing SMC is generally more stable and robust when inductor current and input capacitor voltage are considered as the state variables. Based on this concept and redefining SS as $H := \frac{\partial p}{\partial x_1} = x_2$, the boundary conditions for such region $\mathbf{\Pi}$ derived from (9) and (12) can be defined as

$$\mathbf{\Pi}_1 := x_1 > 0 \quad \text{and} \quad \mathbf{\Pi}_2 := x_1 - x_3 < 0 \tag{15}$$

which is larger than that of region (14). While in case of buck and buck-boost converters, trajectories **B** and **C** (denoted by green and blue curves) without satisfying (13), are intersecting the SS $H = 0$ in finite time. Once they satisfy, just after the first intersection sliding motion starts and trajectories **B** and **C** continue to move toward the equilibrium points. The solution of each motion is unique if switching frequency f_s inside the chatter-box is ideally infinity. However, since in reality, such assumption is not true, the equivalent dynamics of motion derived from Utkin's theory may not be always successful to predict the existence of a unique solution [21]. As reported before, it can only be successfully used if the long time average value of fast-scale oscillation is zero or the MIC systems are stable in fast time-scale.

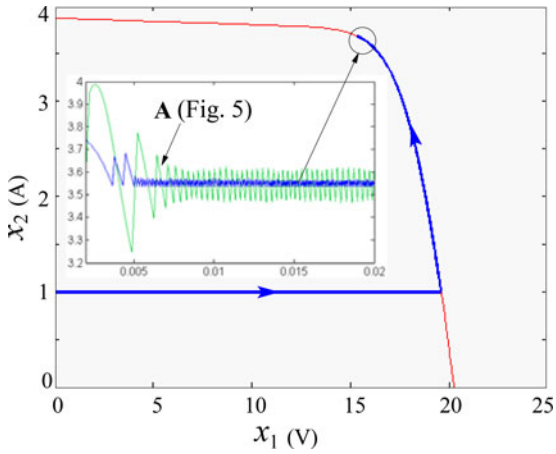

Fig. 6. Performances of boost-type MIC under enhanced existence region $\mathbf{\Pi}$ (represented by shadowed region). The parameters value are: $L = 140\ m$H, $C = 0.1\ \mu$F, and $i_o = 2.3$ A.

B. Prediction of Fast-Scale Stability Margin

In order to investigate such dynamics of MPVS, it is necessary to estimate the fast-scale stability margin at clock speed. It is also necessary to estimate the range of tunable or external parameters that will ensure without onset of chaos. The stability analysis using "complete one cycle fundamental solution matrix"—called monodromy matrix was addressed earlier, to solve this problem [34]. In this approach, the stability of a periodic orbit is determined by using the state transition matrices for the segments of the orbits lying in the individual subsystems, and the transition matrices across the switching—called saltation matrix. Once the monodromy matrix is obtained, the eigenvalues of that matrix determine the stability of the periodic orbit to small perturbation.

To apply this concept, we derive an approximate chattered dynamics inside the switching box S_B by successively linearizing (10) around the MPP as $i_{\rm pv} = I_{\rm mpp} - \beta\,(x_1 - V_{\rm mpp})$, where $\beta = \frac{di_{\rm pv}}{dx_1}|_{x_1 = V_{\rm mpp}} \approx \frac{I_{\rm mpp}}{V_{\rm mpp}}$. Then, substituting it into (9) to form a set of 2-D linear time-invariant (LTI) subsystems[2] as

$$\frac{dx}{dt} = \begin{cases} M_1 : A_1 x + B_1 & \forall\, nT < t < d_n T + nT \\ M_2 : A_2 x + B_2 & \forall\, d_n T + nT < t < (1+n)T \end{cases} \tag{16}$$

where d_n is the steady-state duty ratio (see Fig. 4), and A_i and B_i are the corresponding system and input matrices respectively, as shown in Table III. Having obtained (16) if one assumes $t = nT$ is a switching instant, then the monodromy matrix over complete one cycle T can be expressed as the composition of state transition matrices over the two phases of evolutions M_1 and M_2, and two saltation matrices for the switching from M_1 to $M_2(\mathbf{S_1})$ and back to $M_1(\mathbf{S_2})$ as [34]

$$\mathbf{M} = \mathbf{S_2}\Phi_2\mathbf{S_1}\Phi_1 \tag{17}$$

[2]Since in local neighborhood of MPP the chattered dynamics is much faster than x_3; it is, therefore, reasonable to consider $x_3 = V_o$ and $dx_3/dt = 0$.

TABLE III
SYSTEM AND INPUT MATRICES A_i AND B_i

Buck : $A_1 =$ $\begin{bmatrix} \frac{-\beta}{C} & 0 \\ 0 & 0 \end{bmatrix}$	$A_2 =$ $\begin{bmatrix} \frac{-\beta}{C} & \frac{-1}{C} \\ \frac{1}{L} & 0 \end{bmatrix}$	$B_1 = B_2 =$ $\begin{bmatrix} \frac{2I_{\rm mpp}}{C} \\ \frac{-V_o}{L} \end{bmatrix}$	
Boost : $A_1 = A_2 =$ $\begin{bmatrix} \frac{-\beta}{C} & \frac{-1}{C} \\ \frac{1}{L} & 0 \end{bmatrix}$	$B_1 =$ $\begin{bmatrix} \frac{2I_{\rm mpp}}{C} \\ \frac{-V_o}{L} \end{bmatrix}$	$B_2 =$ $\begin{bmatrix} \frac{2I_{\rm mpp}}{C} \\ 0 \end{bmatrix}$	
Buck-boost : $A_1 =$ $\begin{bmatrix} \frac{-\beta}{C} & 0 \\ 0 & 0 \end{bmatrix}$	$A_2 =$ $\begin{bmatrix} \frac{-\beta}{C} & \frac{-1}{C} \\ \frac{1}{L} & 0 \end{bmatrix}$	$B_1 =$ $\begin{bmatrix} \frac{2I_{\rm mpp}}{C} \\ \frac{V_o}{L} \end{bmatrix}$	$B_2 = \begin{bmatrix} \frac{2I_{\rm mpp}}{C} & 0 \end{bmatrix}^T$

where $\Phi_1 = e^{A_1 d_n T}$ and $\Phi_2 = e^{A_1(1-d_n)T}$ are the state transition matrices. $\mathbf{S_1}$ and $\mathbf{S_2}$ are the saltation matrices represented by

$$\mathbf{S_1} = \mathbf{I} + \frac{[(A_2 - A_1)x + (B_2 - B_1)]\nabla H}{\nabla H(A_1 x + B_1) + \frac{dH}{dt}}\bigg|_{t = d_n T} \tag{18}$$

and $\mathbf{S_2} = \mathbf{I}$, an identity matrix. However, to evaluate such matrices one needs to know the duty ratio d and corresponding state vectors at the switching instant $t^* = d_n T$. This can be accurately obtained by using the Newton–Raphson method. Alternatively, one can use any standard simulator to obtain the stable behavior, from which the information about both d_n and $x^*|_{t = d_n T}$ can be extracted. However, from aforementioned LTI state-space representation the duty-ratio information can be extracted easily by solving M_1, as

$$d_n = \underbrace{\frac{C}{\beta T}\ln(1 + \Delta x_1)}_{\text{buck and buck-boost}} \text{ and } d_n = \underbrace{\frac{C}{\beta T}\frac{\Delta x_1}{(1 - x_2^*/I_{\rm mpp})}}_{\text{boost}};\ T \ll 1 \tag{19}$$

where x_2^* is the lower limit of steady-state inductor current, $\Delta x_1 = (V_{\rm mpp} - x_{1n})/V_{\rm mpp}$ is the normalized input capacitor ripple with $x_1^* = V_{\rm mpp}$, and $x_1|_{t=nT} = x_{1n}$. While in calculating $\mathbf{S_1}$, the switching function is $H = x_1 - V_{\rm mpp}$ so that the normal is $\nabla H = [1\ 0]$ and the time derivative is $dH/dt = 0$. Substituting these expressions into (18), we obtain the saltation matrix of buck converter

$$\mathbf{S_1^{\rm buck}} = \begin{bmatrix} 1 - x_2^*/I_{\rm mpp} & 0 \\ C/\beta L & 1 \end{bmatrix}. \tag{20}$$

Similarly, for boost and buck-boost converters it can be easily evaluated as

$$\mathbf{S_1^{\rm boost}} = \begin{bmatrix} 1 & 0 \\ 0 & 1/(1-D) \end{bmatrix} \quad \text{and}$$

$$\mathbf{S_1^{\rm buck-boost}} = \begin{bmatrix} 1 - x_2^*/I_{\rm mpp} & 0 \\ C(1-D)/\beta L & 1 \end{bmatrix}$$

where $D = V_0/V_{\rm mpp}$. Once the saltation matrix and corresponding duty ratios are known, one can easily calculate the monodromy matrix from (17). The monodromy matrix represents

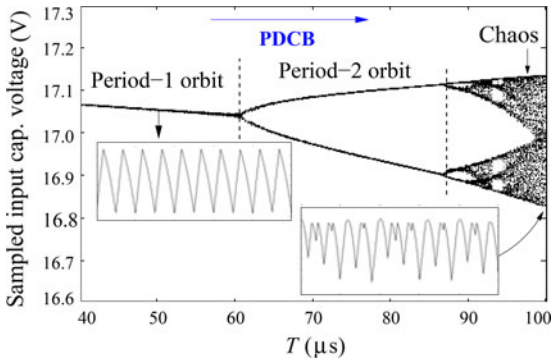

Fig. 7. Representative bifurcation diagram showing the fast-scale instabilities of buck-type MIC for $L = 140\ \mu$H, $C = 1000\ \mu$F, and $i_o = 5.45$ A. Here, T is taken as the bifurcation parameter.

the linearized system integrated around the periodic orbits and, hence, its eigenvalues

$$\lambda_{1,2} = ||\mathbf{M}|| \tag{21}$$

represent the Floquet multipliers. If they lie within the unit circle (i.e., $\lambda_{1,2} < 1$), the orbit is stable and that can be ensured as follows.

C. Design Guidelines

Here, Δx_1 and β are the known parameters and their exact values can be substituted directly into (19) for inspection. However, for designing the circuit parameters such as C, L, and T, it is necessary to consider their maximum or minimum values for ensuring the abidance of nominal period-1 operation. Since at nominal operation $\Delta x_1 \ll 1$ is always held; therefore, baseline design guideline for choosing such C and T should be $C/\beta T \gg 1$, preferably be in the hundred. However, T should not be chosen too high to avoid undesirable high-frequency artifacts, such as switching noise that may cause interfere with controller. In such situation, C may be used in conjunction with T to achieve a large value of $C/\beta T$, so that the condition $d_n := \frac{C}{\beta T} \ln(1 + \Delta x_1) < 1$ is satisfied. While in case of L, one should choose its value sufficiently large in order to ensure the CCM operation (i.e., $x_2^* > 0$) and the stability condition (21). Based on the above guidelines, we select all the components value and investigate the dynamic behavior of the MIC by calculating d_n and $\mathbf{S_1}$; thereby, the $\lambda_{1,2}$ of the monodromy matrix. It is found that (say, for buck converter) d_n just before the instability at $T \approx 59\ \mu$s is 0.3711, and corresponding eigenvalues are -0.9941 and 0.3692—implies the orbit is stable, and that is closely matched with the numerically obtained bifurcation diagram as shown in Fig. 7. It also shows that for a low value of T, the system exhibits stable period-1 orbit. However, as the value of T increases, it becomes unstable at $T \approx 60\mu$s through a smooth period-doubling bifurcation. For further increment of clock period T, period-2 orbit bifurcates again, and finally leads to a chaotic orbit through a series of period-doubling-cascade bifurcation (PDCB) in close succession—where the application of Utkin's equivalent control theory is not valid [21]. Moreover, it is important to note that, although such control concept is applicable for high-periodic orbits, but it needs a multiparametric bifurcation diagram to ensure the domain of existence of a periodic operation, which is again undesirable. Therefore, we only consider the period-1 mode of operation for safe operating condition, and that can be explicitly obtained from (19) to (21). In such situation, Filippov's method and Utkin's equivalent control concept can be successfully used to derive the equivalent dynamics of the motion. The idea behind such concepts is that in the vicinity of the sliding surface the velocity vector is always tangential to the sliding surface and the resulting equivalent dynamics of (9) is only governed by a smooth control law without any discontinuity [20].

D. Equivalent SMC and Dynamics of Equivalent Motion

Based on this principle, the equivalent dynamics can be determined by replacing the discontinuous control $u \in (0, 1)$ to an equivalent continuous one $u_{\rm eq}$, which is derived from $\frac{dH}{dt} = 0$ as

$$u_{\rm eq} = -[\nabla H g]^{-1} \nabla H f$$

where $\nabla H g$ is the nonsingular square matrix. After substituting $u_{\rm eq}$ into (9), the equivalent dynamics of buck, boost, and buck–boost converters are obtained as

$$\frac{dx}{dt} = \begin{cases} \begin{bmatrix} 0 & \dfrac{x_1 i_{pv} - x_2 x_3}{x_2 L} & \dfrac{x_2 - i_0}{C_o} \end{bmatrix}^T \\ \begin{bmatrix} \dfrac{i_{pv} - x_2}{C} & 0 & \dfrac{x_1 x_2 - x_3 i_o}{x_3 C_o} \end{bmatrix}^T \\ \begin{bmatrix} 0 & \dfrac{i_{pv}(x_1 - x_3)}{x_2 L} + \dfrac{x_3}{L} & \dfrac{i_{pv} - x_2 - i_0}{C_o} \end{bmatrix}^T \end{cases} \tag{22}$$

which is a nonlinear function of x_1. Once there is a nonlinearity, there may exist more number of feasible equilibrium points and system may converge to some undesirable operating points. For example, see curve $\mathbf{D}$ in Fig. 5. Theoretically, such equilibrium points and their domain of attractions could be successfully eliminated by properly designing the MPVSs, and also identifying their stable operating regions using stable- and unstable manifolds-based large-signal stability analysis [35]. This paper, however, deals to design the system by satisfying existence condition (13). It is found that if the equivalent sliding motion inside the stable region does not cross the limiting boundary $\Pi_1 = i_{\rm pv}$ as $t \to \infty$ (i.e., if the existence condition is not violated), then the system is stable. This can occur only when inductor current x_2 (for buck converter load current $i_{\rm o}$) becomes just greater than that of the MPP current $I_{\rm mpp} = i_{\rm pv}|_{\rm mpp}$, i.e.,

$$\mathbf{\Pi} : x_2 \geq I_{\rm mpp}. \tag{23}$$

The condition (23) is quite general and true for all switching converters, when there exists a finite existence region defined by (13) and (14). However, due to different converters' topological configurations and switching function formulation, the stability region satisfying the aforementioned existence condition may also vary. For instance, the buck converters are conditionally stable and that stability region (also called MPP region [4]) is strongly limited by their minimum loading

condition $I_o = I_{mpp}$. This can also be verified by solving (22) as $(X_2/i_{pv})|_{mpp} = (X_1/X_3) > I_{mpp}$, where $X = [X_1\ X_2\ X_3]^T$ are steady-state equilibrium point. Although such limitation can be solved by using buck-boost converters (since $I_{mpp} < X_2 := (1 - X_1/X_3)\, i_{pv} < I_{mpp}$), but they requires extra hardware circuitries to invert their output voltages. While the main disadvantages of noninverting buck-boost topology are the increased number of controllable switches and inductors [4], more complex control solution [19], and the achievable conversion efficiency, which is typically lower than the buck or boost converter for the same rating. In contrast, the boost converter is an attractive choice because of its ability to increase the output voltage (requiring fewer panels for a given desired output voltage), but main disadvantage is its limited operating region. The output current of boost converter can never be higher than the input current, the range over which current mismatch can be addressed is severely limited [1], [3], [36]. Regardless of the control algorithms used, it is always true for boost converters, and it can also be easily validated from reduced-order dynamics (22) as $X_2 = (X_3/X_1)I_o \le I_o$, where $X_2|_{mpp} := I_{mpp}$.

Therefore, it can be concluded that the aforementioned concepts provide a simple way for the circuit designer to select the parameters for successful operation of ASMC. Given certain specifications, the designer would first roughly set the range of circuit parameters and load in a conventional way based on (22). This gives the desired slow time-scale stability and transient performance, but will not guarantee that the system will be stable on a fast time-scale. In order to ensure the nominal period-1 operation, it will be necessary to calculate the range of storage elements and switching frequency for which the period-1 orbit will remain stable. The designer will have to ensure that the circuit parameters simultaneously satisfy the conditions (21) and (23). Once it is satisfied, the equivalent motion (22) always exists and solution of that motion is unique.

IV. Performance Analysis and Its Experimental Validation

A. Realization of ASMC-Based MPPT

To investigate the effectiveness in terms of efficiency and dynamic performances, the concept has been analyzed numerically as well as experimentally (see Fig. 8) using buck-type MIC. The synchronous buck topology enables both high-switching frequency (important for low cost, small size) and high efficiency, it does not contribute any voltage gain (which would reduce the number of panels that must be series connected). In most utility-based and residential installations, however, there are a sufficient number of PV panels to provide for the inherent stacking of voltages without requiring the additional step-up from the power converter. When not tasked with providing additional voltage step-up, the power stage can be optimized for cost, size, and efficiency [3].

Nevertheless, the control law $\text{sign}(\dot{v})\text{sign}(\dot{p})$ of (6), which is applicable for all converter topologies can be implemented by applying only a few commonplace analog components. The signals after sensing are successively fed to an analog multiplier **AD633** which is utilized to assess the array power $p = vi_{pv}$ and

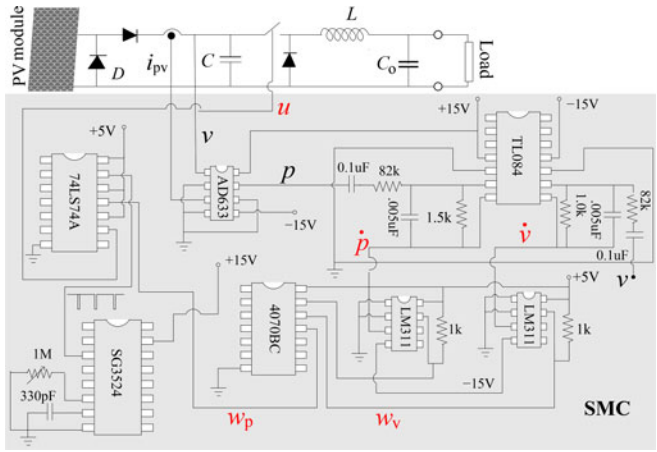

Fig. 8. Schematic diagram of indoor test set-up.

then, to a differentiator which is realized by a first-order high-pass filter with an arbitrarily chosen time constant $T_d \approx 100\ \mu$s (since perfect differentiators cannot be realized in practice). Note that, its output yields only an approximation to the true time derivative of both p and v. Moreover, instead of using ± 1 to represent the sign of $\dot{p}$ or $\dot{v}$, it is more convenient in practice to use the boolean 0/1. A comparator **LM311** is used to evaluate the sign of $\dot{p}$ by producing a binary signal w_p, whose value is 0 if $\dot{p} < 0$ or 1 if > 0. The array voltage v is also treated likewise and produces a second binary signal w_v. The multiplication of these signals (using XOR gate **4070BC**) gives another binary signal, which would indicate whether v should be increased or decreased in order to converge upon the MPP. If its output is 0, then v should be increased, else if 1, then v should be decreased. This is obtained by feeding the sampled output of XOR-gate to a D-type latch **74LS74** so that the output of the latch circuit provides a signal that makes a decision to close or open the switch only at regular intervals. Moreover, the latch circuit minimizes the effects of unavoidable interference generated by the converter's switching action, and likewise prevents the high-frequency chattering within the switching box S_B. Thus, the controller acts as a Δ-neighborhood SMC (see Section II).

B. Performance Analysis

In an ideal SMC, the total time taken to complete both the SM operation phase and the reaching phase is known as settling time t_s [32]. Depending on the magnitude of load and irradiation fluctuations, the capacity of C, L, and C_o, the time taken for x to track from any point on $H = 0$ to the steady-state equilibrium may vary. Under parameter fluctuation, the resulting t_s will be small if x reaches SS within the existence region $\mathbf{\Pi}$. This can be explained by a representative phase-plane diagram as shown in Fig. 9(a). Here, for irradiance $G = 1000$ W/m^2 and an arbitrary initial condition x eventually hits H, inside the existence region $\mathbf{\Pi}_{1000}$ in finite time and slides along the surface. Once we change G from 1000 to 400 and then to 30 W/m^2 successively, the trajectory suddenly starts from a different initial position (which is the final value of the previous states) and reaches $H = 0$, inside the region $\mathbf{\Pi}_{400}$ and $\mathbf{\Pi}_{30}$, respectively. Since it

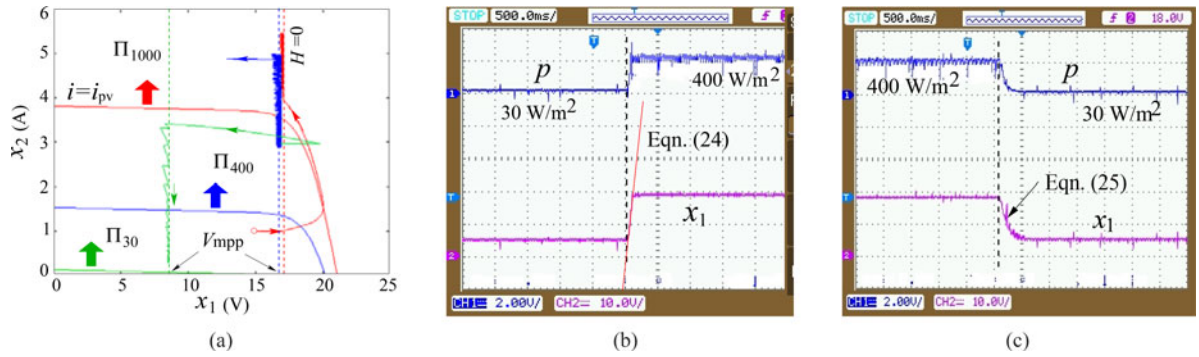

Fig. 9. (a) Condition for less transient oscillation under sudden irradiation variation from 1000 to 400, and then, from 400 to 30 W/m^2; and corresponding experimental validation for irradiation fluctuations: (b) from 30 to 400 and (c) from 400 to 30 W/m^2. CH 1: p (18 W/div), CH 2: v (10 V/div). All other parameters are same as in Fig 5.

reaches the switching surface within the existence regime, one could expect a less oscillatory dynamic responses during the reaching phase, and that can be evaluated from (9) as

$$x_1 = \frac{i_{\rm pv}(G+\Delta G) - i_{\rm pv}(G)}{C} t \tag{24}$$

where ΔG is the step-up irradiation fluctuation. While for step-down irradiance, trajectory evolution from one attracting region to another is governed by third-order dynamical equation[3]

$$C_o L \frac{d^3x_1}{dt^3} + \frac{L}{R_{\rm eq}} \frac{d^2x_1}{dt^2} + \left(1 + \frac{C_o}{C}\right) \frac{dx_1}{dt} + \frac{1}{CR_{\rm eq}} x_1 = \frac{V_{\rm bus}}{R_{\rm eq}} + i_{\rm pv} \tag{25}$$

with roots of the characteristic equation $s_{1,2,3} = -1/R_{\rm eq}C_0$, $\pm j\sqrt{(1/LC)}$ for $C_o \gg C$. Moreover, for $\frac{1}{2\pi}\sqrt{(1/LC)} \gg T$, since the natural frequency of oscillation of MPVS is almost constant as compared with an external clock pulse T, therefore, trajectory will be converged exponentially as $x_1(t) = x_1(0)e^{-t/R{\rm eq}C_0}$. This has also been experimentally confirmed by obtaining the continuous-time waveforms of both p and x_1 as shown in Fig. 9(b) and (c). The experimental results are captured by considering a single MPVS with a varying irradiance ranging from 40% to 3% of nominal irradiance $G = 1000$ W/m^2. The classical P&O algorithm and analog ripple correlation control (RCC) [39] techniques with local resistive load 2 Ω are considered to compare the tracking performance for equal irradiation fluctuation, because of their simplicity and easy to implement. Fig. 10 shows that under sudden irradiation fluctuation and CCM operation the ASMC-based MPP tracker not only exhibits a smaller maximum peak over- and under-shoot without loosing the steady-state performance or robustness of the system, but also takes less than 2 ms to settle, which is quite faster than that of adaptive P&O algorithm with step-size Δd [6]. In the past, various digital as well as analog MPPT techniques and their comparative studies have been reported [6], [40], [41]. The careful observations (see Table IV) on such techniques reveal that the adaptive and PI-based P&O techniques are beneficial for

[3]Here, load current $i_{\rm o}$ is approximated as $(v_{\rm o} - V_{\rm bus})/R_{\rm eq}$ [26].

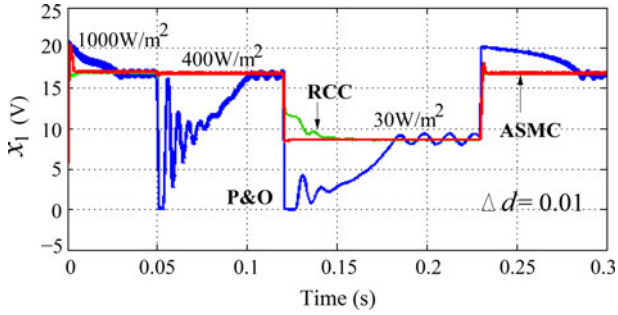

Fig. 10. Tracking performance under sudden change of G.

their high-quality tracking factor (TF), smaller ripple voltage in steady state, good transient performance, and medium complexity of implementation. Nevertheless, since they are implemented in the digital domain (in a microcontroller or FPGA platform), they therefore require more computation time (CT) and results in the closed-loop system to exhibit quantization-induced limit cycle oscillations [13]. Moreover, analog RCC [39] techniques used to deliver maximum available power in the steady state is also not suitable enough (see Fig. 10). Since the MPP of PV system will vary as solar insolation varies, it is not guaranteed that RCC can exhibit critically damping behaviors under rapidly changing environmental conditions. Recently, adaptive RCC technique [23] has demonstrated fast convergence and high performance under rapidly changing weather conditions, but the implementation of this technique can still be undesirably complex. While the proposed ASMC-based MPPT technique is very easy to implement in the analog domain, absolutely free from processing delay and quantization effect, and the cross-coupling effects in case of series-connected converters configuration. Also, it can swiftly converge to the desired MPP with fast dynamic response and guaranteed stability without incorporating any extra hardware complexity.

In order to address these, let us look at (1) and (23). Here, the inequality condition (23) necessarily provides the sufficient condition for an asymptotic stability of the single MPVS. For a fixed value of output voltage and maximum input power $P_{\rm in}|_{\rm mpp} = x_1 i_{\rm pv}|_{\rm mpp}$ [see Fig. 1(b)], the stable steady-state operation of each MPVS is strongly limited by its minimum

TABLE IV
MAJOR CHARACTERISTICS OF MPPT TECHNIQUES

Methods	Tracking Factor	Convergence Time	Steady-State Oscillation	CT and Implementation	Accurate?
P&O [14]	Good	Varies	Varies	Less, Simple	Yes
Adaptive P&O [6]	Very good	Fast	Less	More, Complex	Yes
PI-based P&O	Excellent	Varies	Varies	More, Medium	Yes
InC [37]	Good	Medium	Less	More, Medium	Yes
Laod i_o/v_o maximization [38]	Good	Fast	Varies	More, Medium	No
RCC [39]	Good	Varies	Less	Nil, Simple	Yes
Adaptive RCC [23]	Excellent	Fast	Less	More, Complex	Yes
Proposed ASMC	**Excellent**	**Very Fast**	**Less**	**Nil, Simple**	**Yes**

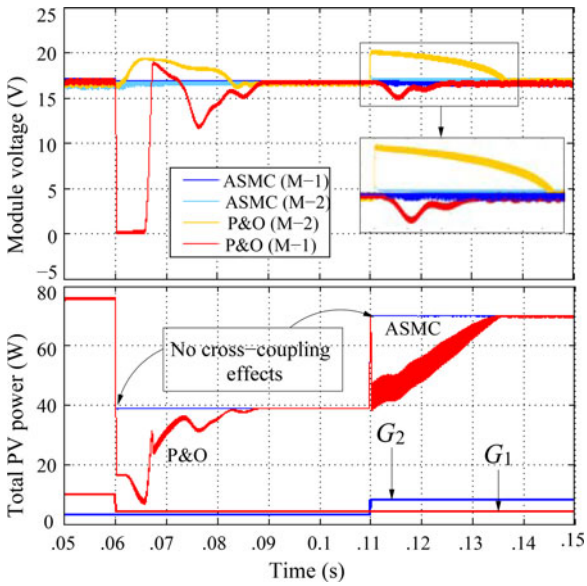

Fig. 11. Dynamic response showing the comparison of coupling effects between Fig. 1 and P&O-based control algorithm for $i_o = 4.8$ A. Here, G_1 and G_2 represent the solar insolations for first and second module, denoted by M-1 and M-2, respectively.

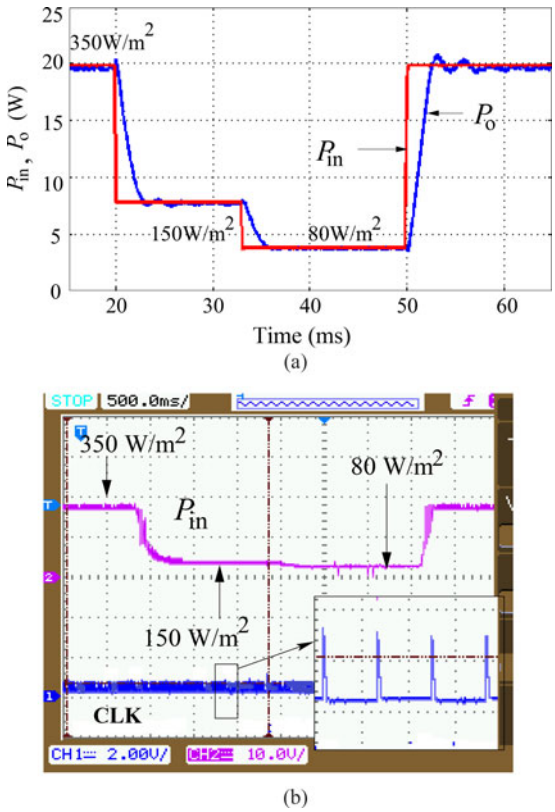

Fig. 12. (a) Representative diagram showing the transient performances of P_{in} and P_o^d (without any cross-coupling effects) for $i_o = 4.8$ A and $R_{eq} = 0.02\ \Omega$ and (b) its experimental confirmation. CH 1 is the clock pulse and CH 2 is the input power $P_{in} \approx 9$ W/div.

loading condition $I_o \leq I_{mpp}$. One cannot operate it satisfactorily over a wide load range. Therefore, in order to balance the input power with its load power, MPVS may operate at some equilibriums which are not the desired MPP [35] (see curve **D** of Fig. 5). However, this can be easily reduced by a series-connected MPVSs architecture[3], [4]. In fact, minimum load current shared by each converter in series configuration will be reduced further than that of single MPVS since $V_{bus} = \sum_1^k V_o^k > V_o^k$ (see Section II). Thus, it essentially interprets as an expanded load range, requirement for the each system's state trajectory or input capacitor voltage to be directed toward respective sliding surface $H^k = (x_1^k - V_{mpp}^k)$ and satisfies the existence condition (23). Once they satisfy, one can expect a stable steady-state operation with fast dynamic response. Moreover, the input voltages of individual modules v^k converge to V_{mpp}^k and remain unaltered over a wide range load variation. Because of this operation proposed MPP tracker forces the MPVS to operate as a voltage source having a small output impedance, and thus gives an insight clue about the cause of reduced cross-coupling effects. The cross-coupling effects are an undesired property of cascaded converter systems, causing reduction in the system power output and dynamic performances [25], [27]. In [25], the authors showed that the reduction of tracking performance due to cross-coupling effects can be significantly improved if the individual converters are closely operated as an ideal voltage source. The mathematical proof of such concept has also been reported therein. With this view, we simulate the series-connected MPVSs and observe the cross-couplings effects by introducing an irradiance sequence (G_1 from 1000 to 500 and G_2 from 400 to 800 W/m^2) into PV modules attached to each converter, while keeping the other parameters' value fixed. Fig. 11 shows that due to slow tracking response of classical P&O algorithm, the dynamic performance of MPPT system under sudden irradiance fluctuation in one module is greatly affected by other one. While in the case of ASMC technique

TABLE V
η (%) OF SERIES CONFIGURATION FOR DIFFERENT G_1 (W/m^2) WHEN $i_o = 4.8$ A AND $R_{eq} = 0.02\ \Omega$

G_1	1000	850	700	550	400	250	50
η	97.52	97.28	96.68	96.66	96.60	96.11	92.76

there are no visible cross-coupling effects. The resulting response in the input voltages of the converters is not affected by the disturbance caused by any changes in other PV module's irradiance. Thus, it improves the energy yield of the system.

Moreover, since the efficiency of the overall system is determined by stable steady-state behavior and transient response of MPPT efficiency [18]; therefore, the highest possible efficiency can only be achieved if the existence condition (23) is satisfied. With this view, system dynamics are analyzed and also validated experimentally over a wide range of rapidly fluctuating irradiances. The test has been performed in indoor by considering a string of two series-connected MPVSs, and each of them is artificially illuminated by different levels irradiances $G_1 = 350$ and $G_2 = 40$ W/m^2 (measured by Pyronometer). We then successively change the insolation level G_1 from 350-to-150-to-80, and back to 350 W/m^2 without varying G_2. Fig. 12(a) and (b) reveals that proposed ASMC-based series architecture not only tracks the true MPP of each module efficiently, but is also able to locate and extract the maximum available power from the PV array under any mismatching conditions (see Table V). One cannot achieve it, simply by iteratively changing the duty ratio of individual dc–dc converter under such rapidly changing inhomogeneous solar irradiances.

V. CONCLUSION

In this paper, an analog circuitry-based fast and robust MPP tracker is proposed for buck, boost, and buck–boost-type modular PV systems. Based on the condition of SM in HDSs, we have derived the exact mathematical models for all such converter systems. We have also discussed how the modeling and analysis can be successfully used to design and extract the best optimized performances (in terms of steady state and transient responses with improved overall systems' efficiency) using the concepts of equivalent control law and fast-scale stability analysis. These are experimentally verified by taking an example of buck-type MIC and compared with P&O-based algorithm. The results demonstrate that under sudden irradiation fluctuations, the tracking performances of analog MPP tracker employing SMC is not only faster than the reference one, but also exhibits less steady-state oscillations with reduced cross-coupling effects. One drawback of this method is that if the converter's switching frequency varies, it is required to redesign the high-pass filter circuit which is used to obtain the time derivatives of module current and voltage. Moreover, hardware realization of boost-type tracker and also its use in cascaded converters architecture is a subject of our current investigation.

REFERENCES

[1] G. R. Walker and P. C. Sernia, "Cascaded DC–DC converter connection of photovoltaic modules," *IEEE Trans. Power Electron.*, vol. 19, no. 4, pp. 1130–1139, Jul. 2004.

[2] A. Bidram, A. Davoudi, and R. S. Balog, "Control and circuit techniques to mitigate partial shading effects in photovoltaic arrays," *IEEE J. Photovoltaic*, vol. 2, no. 4, pp. 532–546, Oct. 2012.

[3] R. C. N. Pilawa-Podgurski and D. J. Perreault, "Submodule integrated distributed maximum power point tracking for solar photovoltaic applications," *IEEE Trans. Power Electron.*, vol. 28, no. 6, pp. 2957–2967, Jun. 2013.

[4] F. Wang, X. Wu, F. C. Lee, Z. Wang, P. Kong, and F. Zhuo, "Analysis of unified output MPPT control in sub-panel PV converter system," *IEEE Trans. Power Electron.*, vol. 29, no. 3, pp. 1275–1284, Mar. 2014.

[5] M. S. Agamy, M. H. Todorovic, A. Elasser, S. Chi, R. L. Steigerwald, J. A. Sabale, A. J. McCann, Li Zang, and F. Mueller, "An efficient partial power processing DC/DC converter for distributed PV architectures," *IEEE Trans. Power Electron.*, vol. 29, no. 12, pp. 674–686, Feb. 2014.

[6] M. A. G. Brito, L. Galotto, Jr, L. P. Sampaio, G. A. Melo, and C. A. Canesin, "Evaluation of the main MPPT techniques for photovoltaic applications," *IEEE Trans. Ind. Electron.*, vol. 60, no. 3, pp. 1156–1167, Mar. 2013.

[7] N. Femia, G. Petrone, G. Spagnuolo, and M. Vitelli, "A technique for improving P&O MPPT performances of double-stage grid-connected photovoltaic systems," *IEEE Trans. Ind. Electron.*, vol. 56, no. 11, pp. 4473–4482, Nov. 2009.

[8] P. E. Kakosimos, A. G. Kladas, and S. N. Manias, "Fast photovoltaic system voltage or current oriented MPPT employing a predictive digital current-controlled converter," *IEEE Trans. Ind. Electron.*, vol. 60, no. 12, pp. 5673–5685, Dec. 2013.

[9] C. W. Chen, K. H. Chen, and Y, M. Chen, "Modeling and controller design of an autonomous PV module for DMPPT PV systems," *IEEE Trans. Power Electron.*, vol. 29, no. 9, pp. 4723–4732, Sep. 2014.

[10] S. Maity and Y. Suraj, "A fixed frequency dual-mode dc–dc buck converter with fast-transient response and high efficiency over a wide load range," in *Proc. Appl. Power Electron. Conf. Expo.*, 2013, pp. 415–420.

[11] S. Maity and Y. Suraj, "Analysis and modeling of a FFHC-controlled dc–dc buck converter suitable for wide range of operating conditions," *IEEE Trans. Power Electron.*, vol. 27, no. 12, pp. 4914–4924, Dec. 2012.

[12] M. Bradley, E. Alarcón, and O. Feely, "Design-oriented analysis of quantization-induced limit cycles in a multiple-sampled digitally controlled buck converter," *IEEE Trans. Circuits Syst. I, Fundam. Theory Appl.*, vol. 61, no. 4, pp. 1192–12–5, Apr. 2014.

[13] R. P. Venturini, V. V. R. Scarpa, G. Spiazzi, and S. Buso, "Analysis of limit cycle oscillations in maximum power point tracking algorithms," in *Proc. Power Electron. Spec. Conf.*, Jun. 2008, pp. 15–19.

[14] N. Femia, G. Petrone, G. Spagnuolo, and M. Vitelli, "Optimization of perturb and observe maximum power point tracking method," *IEEE Trans. Power Electron.*, vol. 20, no. 4, pp. 963–973, Jul. 2005.

[15] V. V. R. Scarpa, S. Buso, and G. Spiazzi, "Low complexity MPPT technique exploiting the PV module MPP locus characterization," *IEEE Trans. Ind. Electron.*, vol. 56, no. 5, pp. 1531–1538, May 2009.

[16] Y. Levron and D. Shmilovitz, "Maximum power point tracking employing sliding mode control," *IEEE Trans. Circuits Syst. I, Fundam. Theory Appl.*, vol. 60, no. 3, pp. 724–732, Mar. 2013.

[17] E. Mamarelis, G. Petrone, and G. Spagnuolo, "An hybrid digital–analog sliding mode controller for photovoltaic applications," *IEEE Trans. Ind. Inform.*, vol. 9, no. 2, pp. 1094–1103, May 2013.

[18] E. Bianconi, J. Calvente, R. Giral, E. Mamarelis, G. Petrone, C. A. Ramos-Paja, G. Spagnuolo, and M. Vitelli, "A fast current-based MPPT technique employing sliding mode control," *IEEE Trans. Ind. Electron.*, vol. 60, no. 3, pp. 1168–1178, Mar. 2013.

[19] E. Mamarelis, G. Petrone, and G. Spagnuolo, "Design of a sliding mode controlled SEPIC for PV MPPT applications," *IEEE Trans. Ind. Electron.*, vol. 61, no. 7, pp. 3387–3398, Jul. 2014.

[20] M. di. Bernardo, C. J. Budd, A. R. Champneys, and P. Kowalczyk, *Piecewise-Smooth Dynamical Syst.: Theory Appl*. Appl. Math. Sci. New York, NY, USA: Springer, 2008.

[21] J. C. Alexander and T. I. Seidman, "Sliding modes in intersecting switching surfaces—II: Hysteresis," *Houston J.Math.*, vol. 25, no. 1, pp. 185–211, 1999.

[22] S. K. Mazumder, A. H. Nayfeh, and D. Boroyevich, "Theoretical and experimental investigation of the fast-scale and slow-scale instabilities of a dc–dc converter," *IEEE Trans. Power Electron.*, vol. 16, no. 2, pp. 201–216, Mar. 2001.

[23] R. Khanna, Q. Zhang, W. E. Stanchina, G. F. Reed, and Z. H. Mao, "Maximum power point tracking using model reference adaptive control," *IEEE Trans. Power Electron.*, vol. 29, no. 3, pp. 1490–1499, Mar. 2014.
[24] J. M. Carrasco, L. G. Franquelo, J. T. Bialasiewicz, E. Gaalvan, R. C. P. Guisado, M. A. M. Prats, J. I. Leon, and N. Moreno-Alfonso, "Power electronics systems for the grid integration of renewable energy sources: A survey," *IEEE Trans. Ind. Electron.*, vol. 53, no. 4, pp. 1002–1016, Jun. 2006.
[25] J. Huusari and T. Suntio, "Origin of cross-coupling effects in distributed dc–dc converters in photovoltaic applications," *IEEE Trans. Power Electron.*, vol. 28, no. 10, pp. 4625–4635, Oct. 2013.
[26] N. Femia, G. Lisi, G. Petrone, G. Spagnuolo, and M. Vitelli, "Distributed maximum power point tracking of photovoltaic arrays: Novel approach and system analysis," *IEEE Trans. Ind. Electron.*, vol. 55, no. 7, pp. 2610–2621, Jul. 2008.
[27] G. Petrone, C. A. Ramos-Paja, G. Spagnuolo, and M. Vitelli, "Granular control of photovoltaic arrays by means of a multi-output maximum power point tracking algorithm," *Prog. Photovolt. Res. Appl.*, vol. 21, no. 5, pp. 918–923, 2013.
[28] N. Famia, M. Fortunato, G. Lisi, G. Petrone, G. Spagnuolo, and M. Vitelli, "Guidelines for the optimization of P&O technique for grid-connected double-stage potovoltaic systems," in *Proc. IEEE Int. Symp. Ind. Electron.*, Vigo, Spain, Jun. 2007, pp. 2420–2425.
[29] K. Ogata, *Morden Control Engineering*. Englewood Cliffs, NJ, USA: Prentice-Hall, 2010.
[30] J. J. Negroni, D. Biel, F. Guinjoan, and C. Meza, "Energy-balance and sliding mode control strategies of a cascade H-bridge multilevel converter for grid-connected PV systems," in *Proc. IEEE Int. Conf. Ind. Technol.*, Mar. 2010, pp. 1155–1160.
[31] Y. H. Lim and D. C. Hamill, "Simple maximum power point tracker for photovoltaic arrays," *Electron. Lett.*, vol. 36, pp. 997–999, May. 2000.
[32] S. Maity, "Dynamics and stability issues of a discretized sliding-mode controlled dc–dc buck converter governed by fixed-event-time switching," *IEEE Trans. Circuits Syst. I, Fundam. Theory Appl.*, vol. 60, no. 6, pp. 1657–1669, Jun. 2013.
[33] E. J. Brea, A. S. Llinas, E. O. Rivera, and J. G. Llorente, "A maximum power point tracker implementation for potovoltaic cells using dynamic optimal voltage tracking," in *Proc. 25th Annu. IEEE Appl. Power Electron. Conf. Expo.*, Feb. 2010, pp. 2161–2165.
[34] D. Giaouris, S. Maity, S. Banerjee, V. Pickert, and B. Zahawi, "Application of Filippov method for the analysis of subharmonic instability in dc–dc converters," *Int. J. Circuit Theory Appl.*, vol. 37, no. 8, pp. 899–919, 2009.
[35] B. H. Cho, J. R. Lee, and F. C. Y. Lee, "Large-signal stability analysis of spacecraft power processing systems," *IEEE Trans. Power Electron.*, vol. 5, no. 1, pp. 110–116, Jan. 1990.
[36] R. Alonso, E. Román, A. Sanz, V. E. M. Santos, and P. Ibáñz, "Analysis on inverter-voltage influence on distributed MPPT architecture performance," *IEEE Trans. Ind. Electron.*, vol. 59, no. 10, pp. 3900–3906, Oct. 2012.
[37] A. Safari and S. Mekhilef, "Simulation and hardware implementation of incremental conductance MPPT with direct control method using Cuk converter," *IEEE Trans. Ind. Electron.*, vol. 58, no. 4, pp. 1154–1161, Apr. 2011.
[38] Y Jiang, J. A. A. Qahouq, and T. A. Haskew, "Adaptive step size with adaptive-perturbation-frequency digital MPPT controller for a single-sensor photovoltaic solar system," *IEEE Trans. Power Electron.*, vol. 28, no. 7, pp. 3195–3205, Jul. 2013.
[39] T. Esram, J. W. Kimball, P. T. Krein, P. L. Chapman, and P. Midya, "Dynamic maximum power point tracking of photovoltaic arrays using ripple correlation control," *IEEE Trans. Power Electron.*, vol. 21, no. 5, pp. 1282–1291, Sep. 2006.
[40] F. Zhang, K. Thanapalan, A. Procter, S. Carr, and J. Maddy, "Adaptive hybrid maximum power point tracking method for a photovoltaic system," *IEEE Trans. Energy Convers.*, vol. 28, no. 3, pp. 353–360, Jun. 2013.
[41] T. Esram and P. L. Chapman, "Comparison of photovoltaic array maximum power point tracking techniques," *IEEE Trans. Energy Convers.*, vol. 22, no. 2, pp. 439–449, Jun. 2007.

Somnath Maity (M'11) received the M.Tech. degree from the Indian Institute of Technology, Madras, India, in 2003 and the Ph.D. degree from the Indian Institute of Technology, Kharagpur, India, in 2009.

He is currently an Assistant Professor with the Department of Electrical Engineering, National Institute of Technology, Rourkela, India. His research interests include nonlinear dynamics of power electronic circuits and systems, modeling and analysis of complex engineered systems such as smart grids, hybrid electric vehicles, and dc distributed power systems.

Pradeep Kumar Sahu received the M.Tech. degree in power electronics and drives from the School of Electrical Engineering, KIIT University, Bhubaneswar, Odisha, India, in 2008. He is currently working toward the Ph.D. degree in the Department of Electrical Engineering, National Institute of Technology, Rourkela, Odisha, India.

His current research interests include modeling and control of power electronic converters, and power quality improvement in electric distribution systems.